

## Convective motion in collisionless trapped electron mode turbulence

Y. Xiao<sup>1,2</sup> and Z. Lin<sup>1,3</sup><sup>1</sup>*Department of Physics and Astronomy, University of California, Irvine, California 92697, USA*<sup>2</sup>*Institute for Fusion Theory and Simulation, Zhejiang University, Hangzhou 310027, China*<sup>3</sup>*Fusion Simulation Center, Peking University, Beijing 100871, China*

(Received 4 August 2011; accepted 20 October 2011; published online 28 November 2011)

Global gyrokinetic particle simulation of collisionless trapped electron mode turbulence in toroidal plasmas finds both diffusive and convective electron motion using a Lagrangian analysis. The convective motion is identified using simulation and analytic theory to arise from the conservation of the second invariant when resonant trapped electrons lose kinetic energy to the drift wave. A resonance broadening model fits well the diffusive and convective electron motion. © 2011 American Institute of Physics. [doi:10.1063/1.3661677]

Collisionless trapped electron mode (CTEM) turbulence<sup>1</sup> is a prominent candidate for the anomalous transport observed in high temperature fusion plasma. Understanding the transport mechanism of CTEM is critical to improve the electron confinement<sup>2–4</sup> of a burning plasma such as ITER (Ref. 5) where the energetic  $\alpha$ -particles will mostly heat electrons. Recently, the large scale gyrokinetic particle simulation has emerged as a major tool to study the CTEM turbulent transport.<sup>6,7</sup> A latest study finds that the electron transport contains a significant non-diffusive/ballistic component, which is due to the weak detuning of the toroidal precessional resonance and the existence of mesoscale turbulence eddies.<sup>8</sup> This nondiffusive component was further confirmed by the non-Gaussian statistics of the electron heat fluxes.<sup>9</sup> However, the kinetic origin of this non-diffusive component remains elusive. In this letter, we identify the existence of a convective motion of the trapped electrons in the CTEM turbulence by a Lagrangian analysis.<sup>10</sup> Our gyrokinetic simulation and analytic theory find that this convection effect arises because of the conservation of the second invariant for the trapped electrons. The electron phase diagram is made for both convection and diffusion motion in the velocity space, which shows that the convection motion could be important for both deeply trapped and barely trapped electrons, while the diffusion is dominated by the deeply trapped electrons. A resonance broadening model is found to fit well for the diffusion motion and reasonably well for the convection motion.

*Simulation description*—We carried out a gyrokinetic particle simulation using the GTC code<sup>11</sup> to study the CTEM turbulence based on the following parameters:<sup>9</sup>  $R_0 = 1.86 m$ ,  $B_0 = 1.91 T$ ,  $T_e = 2.5 keV$ ,  $n_e = 1.46 \times 10^{20} m^{-3}$ ,  $R_0/L_{Te} = 6.9$ ,  $R_0/L_{Ti} = 2.2$ ,  $R_0/L_n = 2.2$ ,  $a = 250\rho_i$ ,  $a/R_0 = 0.358$ ,  $T_i = T_e$ ,  $m_i/m_e = 1837$ , and the safety factor  $q = 0.58 + 1.09r/a + 1.09(r/a)^2$ , with magnetic shear  $s \equiv d \ln q / d \ln r = 0.78$  at  $r = 0.5a$ . The ion gyroradius  $\rho_i = v_i/\Omega_i$ , where  $v_i = \sqrt{T_i/m_i}$ . A circular cross section model is used for the equilibrium magnetic field,  $B = B_0/(1 + r \cos \theta/R_0)$ , with the simulation carried out in the annulus between  $r = 0.1a$  and  $r = 0.9a$ . The ion is treated by the gyrokinetic equation<sup>12</sup> and electron by an electrostatic version of the fluid-kinetic hybrid model.<sup>13</sup> The electron heat

flux  $q_e$  is represented by an effective heat conductivity  $\chi_e$  using the simple relation  $q_e = n_0 \chi_e \nabla T_e$ , although it will be clarified later that a more appropriate expression for the heat flux includes both a diffusive and a convective term. The heat conductivity  $\chi_e$ , and the volume averaged turbulence amplitude ( $|\delta\phi| = \sqrt{\langle \delta\phi^2 \rangle}$ ) are shown in Fig. 1(a). After an initial exponential growth driven by the CTEM instability, the turbulent transport saturates at a level of gyroBohm diffusivity  $\chi_{GB} = \rho_i^2 v_i/a$ . However, there is a transient period at  $t \in [20, 60]R_0/v_i$ , where the turbulence amplitude is not fully saturated. The turbulence amplitude is fully saturated in the following period of  $[60, 100]R_0/v_i$ , which is sufficiently long to cover all physical time scales relevant to the turbulent transport dynamics.<sup>8</sup>

*Lagrangian analysis*—In the simulation, over  $1.4 \times 10^6$  self-consistent electron markers are tracked, which are selected from the initially loaded Maxwellian. These selected electrons initially stay in a very thin annulus centered at  $r = 0.5a$  with a width less than one typical eddy size<sup>9</sup> and are uniformly distributed in the toroidal direction and in the 2D phase space  $(\lambda, E)$ , with the kinetic energy  $E = m_e v^2/2$  at  $t = 0$  and the other velocity variable  $\lambda = \mu B_0/E$  related to pitch angle.<sup>14</sup> There are about 3200 particles tracked at each phase grid point, which can effectively reduce the Monte Carlo sampling noise. We note that these electrons are actually the self-consistent markers in the particle simulation. Since  $\lambda \in [1 - \varepsilon, 1 + \varepsilon]$  for trapped electrons, the value of  $\lambda$  varies from 0.82 to 1.18 according to the initial value  $\varepsilon = 0.18$ . The value of  $E$  is chosen to vary from 0 to 6  $T$ , with  $T = T_e$ . There are 9 grids in  $\lambda$  and 24 grids in  $E$  altogether. The grid point value is chosen to be the center value at each grid interval. In order to trace the particle, an additional integer is added as the particle label so that we can obtain the exact trajectory for each marker in the simulation. At each grid point in the  $(\lambda, E)$  phase space, we compute the mean radial drift  $\Delta r$  and diffusion  $\Delta r^2$  for these self-consistent markers at each time step by:

$$\Delta r(t) = \frac{1}{N} \sum_{i=1}^N \delta r_i(t) \equiv \langle \delta r_i(t) \rangle, \quad (1)$$

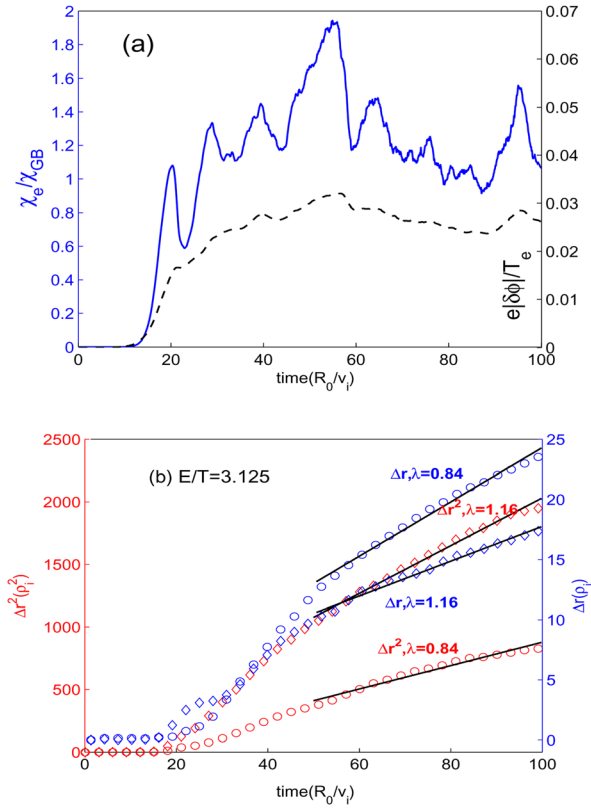


FIG. 1. (Color online) (a) History of electron heat conductivity  $\chi_e$  and turbulence amplitude, averaged over  $r \in [0.37, 0.63]a$ . (b) History of mean radial excursion  $\Delta r$  and diffusion  $\Delta r^2$  for typical barely trapped electron  $\lambda = 0.84$  and deeply trapped electron  $\lambda = 1.16$  at  $E/T = 3.125$ .

$$\Delta r^2(t) = \frac{1}{N} \sum_{i=1}^N (\delta r_i(t) - \langle \delta r_i(t) \rangle)^2, \quad (2)$$

where  $\delta r_i(t) = r_i(t) - r_i(0)$ , and  $i$  is the particle label. As shown by Fig. 1(b), both  $\Delta r$  and  $\Delta r^2$  increase with time, and the trapped electrons possess a radially outward drift. A linear fit of these two quantities in the fully saturated turbulence gives the convection velocity  $v_p$  and the diffusion coefficient  $D$ :  $v_p = \Delta r / \Delta t$  and  $D = \Delta r^2 / 2\Delta t$ . These two quantities are then computed for each phase space grid, as shown in Figs. 2(a) and 3(a). These results show that both diffusion and convection make significant contribution to the electron transport in the CTEM turbulence. This is in contrast to the ion transport in the ion temperature gradient (ITG) driven turbulence, which is dominated by the diffusive component<sup>15</sup> due to parallel wave-particle decorrelation.<sup>9,16</sup>

**Diffusion**—In Fig. 2(a), for each energy  $E$ , the diffusion is stronger for deeply trapped electrons (larger  $\lambda$ ) than the barely trapped electrons (smaller  $\lambda$ ). For each  $\lambda$ , there is an energy that maximizes the diffusion, which is found to be the kinetic energy that gives rise to the precessional resonance. The toroidal precessional frequency of a trapped electron in the large aspect ratio limit is given by<sup>17</sup>

$$\omega_{pres} = \frac{v_i}{R_0} \frac{q\rho_i}{r} (2 - \lambda) \frac{2E}{T_i} \left[ \frac{\mathbf{E}(k)}{\mathbf{K}(k)} - \frac{1}{2} + 2s \left( \frac{\mathbf{E}(k)}{\mathbf{K}(k)} + k - 1 \right) \right], \quad (3)$$

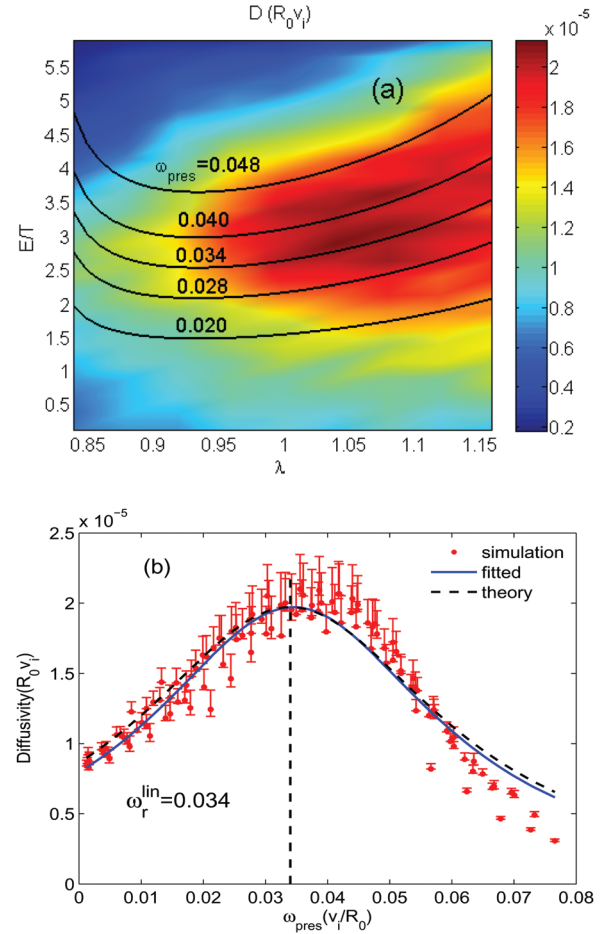


FIG. 2. (a) (Color) Electron diffusion  $D$  in 2D phase space with 9  $\lambda$  grid points and 24  $E$  grid points. Bottom panel (b) Electron diffusion  $D$  vs electron toroidal precessional frequency (red dots), which is fitted by Eq. (4) (solid line). The dashed line is from Eq. (4) by using the theoretical linear eigen frequencies.

with  $\mathbf{K}(k)$  and  $\mathbf{E}(k)$ , the complete elliptic functions and  $k = (1 + \varepsilon - \lambda)/2\varepsilon$ , where  $\varepsilon = r/R_0$  is the inverse aspect ratio, and  $\lambda \in [1 - \varepsilon, 1 + \varepsilon]$  for trapped electrons. The electrons with  $\lambda$  close to  $1 - \varepsilon$  are barely trapped, and those with  $\lambda$  close to  $1 + \varepsilon$  are deeply trapped to the outside of tokamak mid-plane. As Fig. 2(a) shows, the deeply trapped electrons make a dominant contribution to the diffusion process. Since each  $\lambda$  and  $E$  corresponds to a toroidal precessional frequency  $\omega_{pres}$ , we can transfer the 2D diffusion distribution function  $D(\lambda, E)$  in Fig. 2(a) to a 1D function  $D(\omega_{pres})$  in Fig. 2(b) by only counting all the deeply trapped electrons with  $\lambda \in [1.0, 1.16]$  since the contribution from the barely trapped electrons is too small to be significant. The initial values  $q = 1.4$ ,  $s = 0.78$ , and  $r = 0.5a$  are used to calculate  $\omega_{pres}$  by assuming  $q$  and  $s$  do not change much when the particles move radially during this simulation period. As shown in Fig. 2(a), the diffusion is most significant for  $\omega_{pres} \in [0.020, 0.048]$ .

We consider the resonance between the drift wave and the electron banana center executing toroidal precession, which should contribute to most of the diffusion. A Lorentzian distribution based on the resonance broadening formula<sup>18</sup>

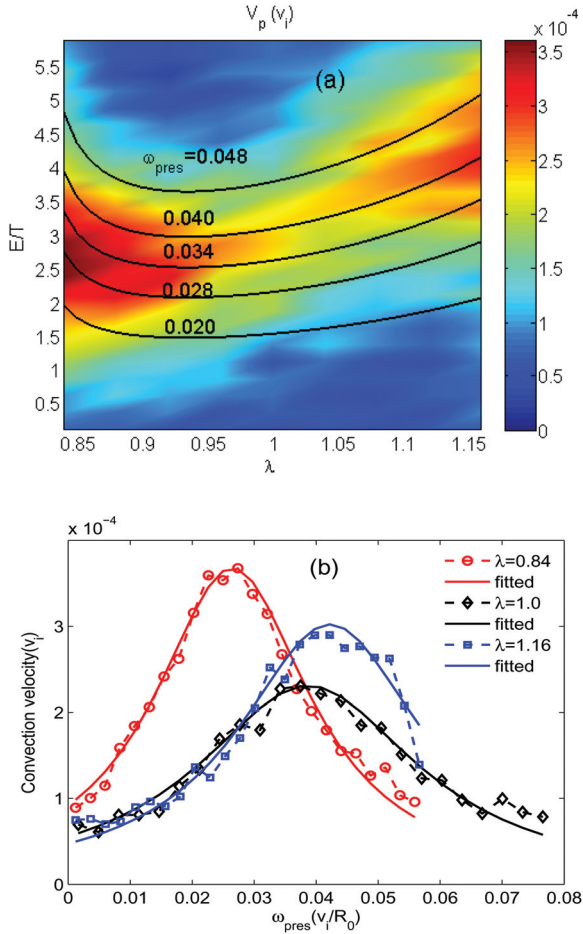


FIG. 3. (a) (Color) Outward convection velocity in 2D phase space. (b) Convection velocity vs electron toroidal precessional frequency for  $\lambda = 0.84, 1.0, 1.16$  and their respective Lorentzian fit by Eq. (4) (solid lines).

$$D(\omega_{pres}) = \frac{D_0 \Delta \omega_{pres}^2}{(\omega_{pres} - \omega_0)^2 + \Delta \omega_{pres}^2} \quad (4)$$

is found to well fit the 1D diffusion distribution  $D(\omega_{pres})$  with  $D_0$ ,  $\omega_0$ , and  $\Delta \omega_{pres}$  the free fitting parameters, which gives  $\omega_0 = 0.0345v_i/R_0$  and  $\Delta \omega_{pres} = 0.0282v_i/R_0$ . On the other hand, the linear eigen frequency of the CTEM instability is dispersiveless,<sup>19</sup>  $\omega_r^{lin} = 1.52k_0\rho_i v_i/R_0$ , which gives  $\omega_r^{lin}/n = 0.034v_i/R_0$  (almost identical to the fitting value  $\omega_0$ !). The nonlinear CTEM turbulence intensity peaks at  $k_0\rho_i \approx 0.35$ ,<sup>9</sup> at which the toroidal mode number  $n \approx 31$  and the linear growth rate  $\gamma^{lin} = 0.21v_i/L_n$ .<sup>19</sup> Therefore,  $\gamma^{lin}/n = 0.030v_i/R_0$ , which is roughly 10% difference from the fitting value  $\Delta \omega_{pres}$ . The dashed line in Fig. 2(b) is Eq. (4) by using the linear eigen frequency  $\omega_r^{lin}/n$  and growth rate  $\gamma^{lin}/n$ . Therefore, the Lorentzian model is accurate to describe the diffusion part of the electron transport in the CTEM turbulence. Note that there is an uncertainty for  $\omega_{pres}$  due to the electron radial movement during measurement, which is accounted for by the error bar in Fig. 2(b). Since there is only a small number of particles at high  $E$  to resolve the velocity space in the simulation, there could have been a large fluctuation for the accuracy of diffusivity at the large  $\omega_{pres}$ , which is not shown by error bar in Fig. 2(b).

*Outward convection*—The 2D contour of Fig. 3(a) shows that there is an outward convection for the trapped electrons in the CTEM turbulence. The barely trapped electrons contribute more to the convection than the deeply trapped electrons. However, the convection velocity does not decrease monotonically with the velocity variable  $\lambda$ . In fact, it first decreases with  $\lambda$  for the barely trapped electrons and increases with  $\lambda$  for the deeply trapped electrons. The deeply trapped electrons feel strongest turbulence intensity due to the ballooning structure of the CTEM turbulence, which represents the force of the turbulence. However, the barely trapped electrons have the smallest bounced averaged inertial, which is the inverse of neoclassical polarization. The combination of these two factors leads to a stronger convection for both barely and deeply trapped electrons than that for the intermediate values of  $\lambda$ . The 2D convection velocity distribution  $V_p(\lambda, E)$  in Fig. 3(a) can be transformed to a 1D distribution function  $V_p(\omega_{pres})$  according to Eq. (3) for different  $\lambda$ . As shown in Fig. 3(b), the distribution function  $V_p(\omega_{pres})$  (the red dots) can be roughly fitted by a Lorentzian of Eq. (4) for each  $\lambda$ . We find that the peak frequency  $\omega_0$  increases with  $\lambda$ , but the spectral width  $\Delta \omega_{pres}$  maximizes at  $\lambda = 1.0$ . The Lorentzian fit of the distribution function  $V_p(\omega_{pres})$  for the barely trapped electrons ( $\lambda = 0.84$ ) gives the peak frequency  $\omega_0 = 0.026v_i/R_0$ , which is lower than the linear eigen frequency  $\omega_r/n = 0.034v_i/R_0$ . The peak frequency for deeply trapped electrons ( $\lambda = 1.16$ ) is fitted to be  $\omega_0 = 0.042v_i/R_0$ , which is higher than the linear eigen frequency. This can also be confirmed by Fig. 3(a), where the curve  $\omega_{pres} = 0.034$  does not exactly go through the peak value of the deeply trapped convection velocities.

The outward convection is found to arise from the conservation of the second invariant  $J_{\parallel} \equiv m_e \oint dl v_{\parallel} = J_{\parallel}(\lambda, E, r)$ , where  $r$  is essentially the banana tip since electron banana width is negligibly small compared to the turbulence eddy size.<sup>9</sup> Since the mode frequency  $\omega$  is smaller than the electron bounce frequency  $\omega_b$ , the second invariant  $J_{\parallel}$  is conserved in the CTEM turbulence. Then  $\Delta J_{\parallel} = 0$  gives

$$\Delta r/R_0 = -F(\lambda, E, r)\Delta E/T_i, \quad (5)$$

with the pinch coefficient  $F(\lambda, E, r) \equiv \frac{T_i}{R_0} \frac{\partial J_{\parallel}/\partial E}{\partial J_{\parallel}/\partial r} \Big|_{\mu, E}$ . Therefore, the convection velocity  $V_p = \frac{d\Delta r}{dt} = -R_0 F(\lambda, E, r) \frac{d}{dt} \left( \frac{\Delta E}{T_i} \right)$ . Thus, the convection velocity is related to the energy change of the electrons. In the CTEM turbulence, the trapped electrons lose kinetic energy to the unstable drift waves, which will introduce an outward convection if the coefficient  $F(\lambda, E, r) > 0$ . Note that the toroidal precessional frequency<sup>20</sup> of trapped electrons  $\omega_{pres} = \frac{q\rho_i v_i}{rT_i} \frac{\partial J_{\parallel}/\partial r}{\partial J_{\parallel}/\partial E} \Big|_{\mu, E}$ , then the convection coefficient is given by a simple relation

$$F(\lambda, E, r) = \frac{q\rho_i}{r} \frac{v_i}{R_0 \omega_{pres}}, \quad (6)$$

with  $\omega_{pres} > 0$  in this normal magnetic shear case ( $s \approx 0.78$ ).

The 2D contour of the energy loss rate ( $-dE/dt$ ) is shown in Fig. 4(a) for each phase grid, which is calculated

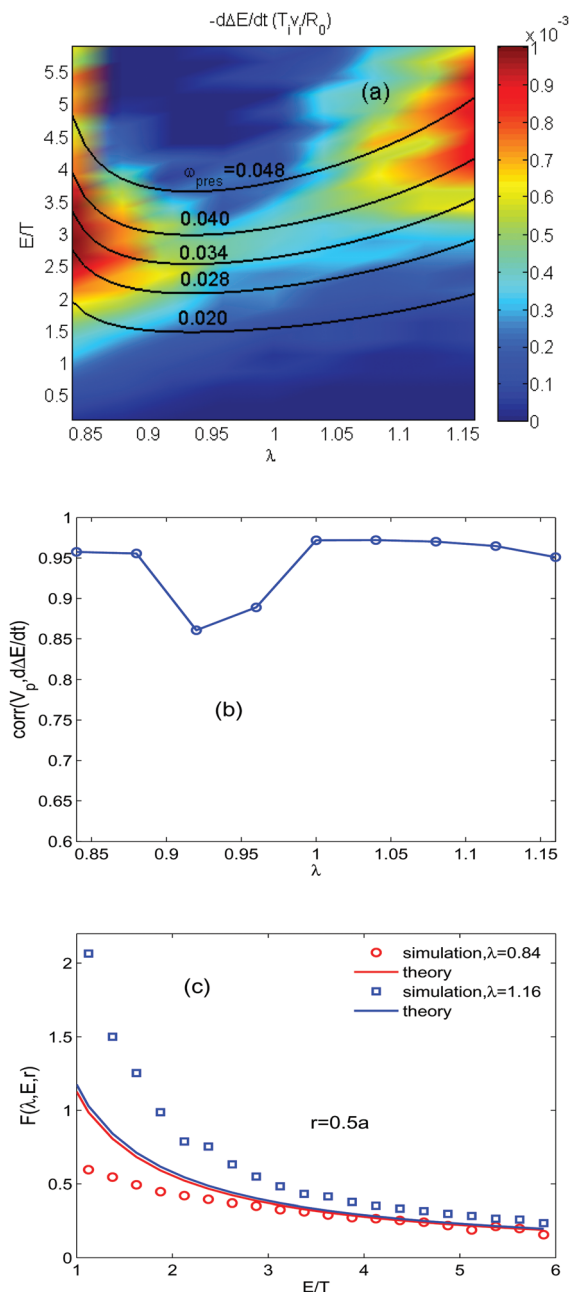


FIG. 4. (a) (Color) Electron energy loss rate in 2D phase space. (b) Cross correlation  $\text{corr}(V_p, d\Delta E/dt)$  between (a) and Fig. 3(a) for different  $\lambda$ . (c) Pinch coefficient  $F(\lambda, E, r)$  vs energy  $E/T$  at  $r = 0.5a$  for deeply and barely trapped electrons, respectively. The discrete diamonds are from the simulation and the solid curves are from analytic formula in Eq. (6).

from the simulation data. Indeed, we see an energy loss for trapped electrons, as it should be. To compare the similarity between Figs. 4(a) and 3(a), we define a cross correlation coefficient for each  $\lambda$ ,  $\text{corr}(X, Y) = \frac{\sum_{i=1}^N X_i Y_i}{\sqrt{\sum_{i=1}^N X_i^2 \sum_{i=1}^N Y_i^2}}$ . This cross correlation coefficient varies from 0 (totally uncorrelated) to 1 (totally correlated). Fig. 4(b) shows that for most  $\lambda$  s, the cross correlation coefficient is greater than 95%. The similarity between Figs. 4(a) and 3(a) further confirms the outward electron convection is due to the loss of electron kinetic energy to the drift waves.

The convection coefficient  $F(\lambda, E, r)$  can be computed from Figs. 3(a) and 4(a), as shown by the discrete markers in

Fig. 4(c) for two typical  $\lambda$  s. The solid curve in Fig. 4(b) is taken from the analytic formula, Eq. (6). The simulation data agree with the theory for both deeply and barely trapped electrons, especially at high energy where the  $E^{-1}$  scaling is directly coming from  $\omega_{pres} \propto E$ . The simulation value is closer to the theoretical value for the barely trapped electron ( $\lambda = 0.84$ ) than for the deeply trapped electron ( $\lambda = 1.16$ ), because the formula for  $\omega_{pres}$  in Eq. (3) is less accurate for deeply trapped electrons and needs finite  $\varepsilon$  correction to the higher order. The discrepancy between the simulation value and theoretical value at low  $E$  is larger for both deeply and barely trapped electrons, because the electron bounce frequency decreases to a level comparable to the mode frequency and the  $J_{\parallel}$  conservation becomes marginal. Therefore, the convective motion of trapped electrons is purely due to the conservation of the second adiabatic invariant  $J_{\parallel}$ , which has been proved by quantitatively comparing simulation and theory. The energy exchange direction between the particle and drift wave, plus the sign of the convection coefficient  $F(\lambda, E, r)$ , determines the direction of the convection.

Similar kinetic mechanism of convection is also likely to occur for the energetic particle transport in the fishbone instability.<sup>21,22</sup>

The work is supported by US DOE SciDac GPS and GSEP centers and an INCITE award, the Fundamental Research Funds for the Central Universities, and the National Magnetic Confinement Fusion Science Program under Grant No. 2011GB105001. The authors are very grateful to L. Chen, I. Holod, and W. Zhang for useful discussions.

<sup>1</sup>W. Horton, *Rev. Mod. Phys.* **71**(3), 735 (1999).

<sup>2</sup>J. C. DeBoo, C. Holland, T. L. Rhodes, L. Schmitz, G. Wang, A. E. White, M. E. Austin, E. J. Doyle, J. Hillesheim, W. A. Peebles, C. C. Petty, Z. Yan, and L. Zeng, *Phys. Plasmas* **17**(5), 056105 (2010).

<sup>3</sup>X. Garbet, L. Garzotti, P. Mantica, H. Nordman, M. Valovic, H. Weisen, and C. Angioni, *Phys. Rev. Lett.* **91**(3), 035001 (2003).

<sup>4</sup>F. Ryter, C. Angioni, A. G. Peeters, F. Leuterer, H. U. Fahrbach, W. Sutrop, and Asdex Upgrade Team, *Phys. Rev. Lett.* **95**(8), 085001 (2005).

<sup>5</sup>ITER. Available from: <http://www.iter.org/>.

<sup>6</sup>R. D. Sydora, V. K. Decyk, and J. M. Dawson, *Plasma Phys. Controlled Fusion* **38**(12A), A281 (1996).

<sup>7</sup>J. Y. Lang, S. E. Parker, and Y. Chen, *Phys. Plasmas* **15**(5), 055907 (2008).

<sup>8</sup>Y. Xiao and Z. H. Lin, *Phys. Rev. Lett.* **103**(8), 085004 (2009).

<sup>9</sup>Y. Xiao, I. Holod, W. L. Zhang, S. Klasky, and Z. H. Lin, *Phys. Plasmas* **17**(2), 022302 (2010).

<sup>10</sup>R. Sanchez, D. E. Newman, J. N. Leboeuf, V. K. Decyk, and B. A. Carreras, *Phys. Rev. Lett.* **101**(20), 205002 (2008).

<sup>11</sup>Z. Lin, T. S. Hahm, W. W. Lee, W. M. Tang, and R. B. White, *Science* **281**(5384), 1835 (1998).

<sup>12</sup>W. W. Lee, *Phys. Fluids* **26**(2), 556 (1983).

<sup>13</sup>Z. Lin, Y. Nishimura, Y. Xiao, I. Holod, W. L. Zhang, and L. Chen, *Plasma Phys. Controlled Fusion* **49**(12B), B163 (2007).

<sup>14</sup>F. L. Hinton and R. D. Hazeltine, *Rev. Mod. Phys.* **48**(2), 239 (1976).

<sup>15</sup>W. L. Zhang, Z. H. Lin, and L. Chen, *Phys. Rev. Lett.* **101**(9), 095001 (2008).

<sup>16</sup>I. Holod and Z. Lin, *Phys. Plasmas* **14**(3), 032306 (2007).

<sup>17</sup>P. Helander and D. Sigmar, *Collisional Transport in Magnetized Plasmas* (Cambridge University, Cambridge, 2005), p. 145.

<sup>18</sup>T. H. Dupree, *Phys. Fluids* **10**(5), 1049 (1967).

<sup>19</sup>G. Rewoldt, Z. Lin, and Y. Idomura, *Comput. Phys. Commun.* **177**(10), 775 (2007).

<sup>20</sup>R. B. White and M. S. Chance, *Phys. Fluids* **27**(10), 2455 (1984).

<sup>21</sup>R. B. White, R. J. Goldston, K. McGuire, A. H. Boozer, D. A. Monticello, and W. Park, *Phys. Fluids* **26**(10), 2958 (1983).

<sup>22</sup>L. Chen, R. B. White, and M. N. Rosenbluth, *Phys. Rev. Lett.* **52**(13), 1122 (1984).